



Research article

A comparative study of ammonia solubility in imidazolium-based ionic liquids with different structural compositions

Muhammad Salman^a, Ji Won Lee^a, Sang Hyuk Lee^a, Min Ho Lee^a, Van Duc Pham^b, Min-Sik Kim^{b,c}, Daeheum Cho^{a,**}, Hye Jin Lee^{a,*}

^a Department of Chemistry and Green-Nano Materials Research Center, Kyungpook National University, 80 Daehakro, Buk-gu, Daegu-city, 41566, Republic of Korea

^b Department of New Biology, DGIST, Daegu, 42988, Republic of Korea

^c New Biology Research Center, DGIST, Daegu, 42988, Republic of Korea

ARTICLE INFO

Keywords:

Imidazolium-based ionic liquids
Thermal stability
Cationic structure
Fluorinated anions
Ammonia solubility

ABSTRACT

Four imidazolium-based ionic liquids (ILs) with two cations 1-pentyl-3-butylimidazolium [PBIM]⁺ and 1-benzyl-3-butylimidazolium tetrafluoroborate [BzBIM]⁺, and two anions tetrafluoroborate (BF₄⁻) and trifluoromethanesulfonate (OTf⁻) were synthesized for NH₃ solubility enhancement. The structural, thermal, and electrochemical stabilities, ionic conductivity, and viscosity of the four ILs, namely, [PBIM]BF₄, [BzBIM]BF₄, [PBIM]OTf, and [BzBIM]OTf, were investigated. Due to the intermolecular interaction of the benzyl group attached to the imidazolium ring, [BzBIM]⁺-based ILs exhibited higher thermal stability but lower ionic conductivity compared to [PBIM]⁺-based ILs. Further, the NH₃ solubility in all ILs was measured using a custom-made setup at temperatures ranging from 293.15 to 323.15 K and pressures ranging from 1 to 5 bar. The effects of the cation and anion structures of ILs, as well as pressure and temperature, on the NH₃ solubility in the ILs were also investigated. [PBIM]BF₄ showed the best solubility because of its high free volume and low viscosity. Density functional calculations validated the superior NH₃ solubility in [PBIM]BF₄, attributable to the minimal reorganization of the [cation]anion complex geometry during the solvation process, yielding a low solvation free energy. The findings of this study suggest that ILs exhibit a high NH₃ solubility capacity and cation and anion structures considerably affect the NH₃ solubility in ILs.

1. Introduction

Ammonia (NH₃) is widely used in various manufacturing industries, particularly as a renewable source for hydrogen production through electrolysis in an alkaline aqueous solution [1,2]. However, such solutions often interfere with the process via H₂O reduction and metallic transport and storage infrastructure corrosions [3]. Therefore, an effective and stable electrolyte with high NH₃ solubility is highly desired. Numerous studies have extensively explored NH₃ solubility in conventional solvents, such as water, acetone, butanol, chlorobenzene, ethylene glycol, methanol, tetrahydrofuran, acetic acid, and mixed solvents [2,4]. For example, ethylene glycol exhibited excellent NH₃ solubility because of the strong interaction between ammonium and the hydroxyl groups of the ethylene glycol

* Corresponding author.

** Corresponding author.

E-mail addresses: daeheumc@knu.ac.kr (D. Cho), hyejinlee@knu.ac.kr (H.J. Lee).

<https://doi.org/10.1016/j.heliyon.2024.e24305>

Received 24 October 2023; Received in revised form 5 January 2024; Accepted 5 January 2024

Available online 6 January 2024

2405-8440/© 2024 The Authors. Published by Elsevier Ltd. This is an open access article under the CC BY-NC-ND license (<http://creativecommons.org/licenses/by-nc-nd/4.0/>).

[2]. A mixed solvent system, incorporating various molar ratios of water and methanol, was also reported to enhance NH_3 solubility [5]. Furthermore, NH_3 solubility in aqueous solutions containing NaCl , NaNO_3 , CH_3COONa , and NaSO_4 has been investigated within the temperature range of 313–393 K [6,7]. NH_3 solubility in aqueous solutions tends to decrease with increasing temperature. This trend, coupled with environmental concerns associated with aqueous NH_3 solutions [7,8], poses challenges such as high vapor pressure, inefficient separation, and NH_3 retrieval difficulty. Overcoming these challenges to achieve NH_3 solubility often requires energy-intensive procedures [8,9].

The aforementioned challenges can be effectively addressed by employing structure-tunable imidazolium-based ionic liquids (ILs) [8–10], which not only offer high NH_3 solubility and selectivity but also facilitate efficient separation and energy-saving procedures. Such ILs exhibit additional advantages, such as high thermal stability, excellent ionic conductivity, wide electrochemical potential windows, and negligible vapor pressure and flammability [3,4,7–9,11–15]. Despite facing challenges such as elevated viscosity, cost inefficiency, environmental toxicity, and non-biodegradability [8,16], imidazolium-based ILs have been the subject of numerous studies exploring NH_3 solubility. For example, Yokozeki et al. investigated NH_3 solubility in four imidazolium-based ILs: namely, 1-butyl-3-methylimidazolium hexafluorophosphate ([BMIM]PF₆), 1-hexyl-3-methylimidazolium chloride ([HMIM]Cl), 1-ethyl-3-methylimidazolium bis(trifluoromethylsulfonyl)imide ([EMIM]Tf₂N), and 1-butyl-3-methylimidazolium tetrafluoroborate ([BMIM]BF₄) [9].

A noteworthy example is the exploration of NH_3 solubility in hydroxyl-functionalized imidazolium-based ILs with diverse anions. The investigation revealed that NH_3 solubility was higher in ILs containing fluorinated anions than in ILs containing nonfluorinated anions. The NH_3 solubility capacity followed the order of $\text{NTf}_2^- > \text{PF}_6^- > \text{BF}_4^- > \text{SCN}^- > \text{NO}_3^-$, attributed to hydrogen bonding between the hydrogen atoms of NH_3 and fluorine atoms in the anions [17]. Moreover, Li et al. investigated the effect of the length of the alkyl chain attached to the imidazolium ring on NH_3 solubility in ILs and revealed that NH_3 solubility is directly proportional to the length [18]. These studies highlight the potentially high NH_3 solubility in imidazolium-based ILs and provide insight into the factors that influence NH_3 solubility in these ILs. Beyond NH_3 solubility studies, imidazolium-based ILs have found applications in the extraction of alkanols from azeotropes [19,20]. A notable example involved the extraction of methanol from a methanol and n-hexane mixture using various imidazolium-based ILs, with 1-butyl-3-methylimidazolium bis(trifluoromethanesulfonyl) exhibiting the highest extraction capacity [21]. Similarly, 2-propanol extraction from azeotropes using ILs was investigated by examining the positive impact of alkyl chain length of imidazolium-based ILs on separation at 298.15 K under atmospheric pressure [22].

In this study, the ILs containing imidazolium cations functionalized with benzyl, pentyl, and butyl groups and fluorinated anions were synthesized, and their NH_3 solubility characteristics were thoroughly investigated. The four investigated ILs were 1-pentyl-3-butylimidazolium tetrafluoroborate ([PBIM]BF₄), [PBIM]OTf, 1-benzyl-3-butylimidazolium tetrafluoroborate ([BzBIM]BF₄), and [BzBIM]OTf. The successful synthesis of these ILs was confirmed using high-resolution mass spectrometry (HR-MS), Fourier-transform infrared spectroscopy (FT-IR), and also proton nuclear magnetic resonance spectroscopy (¹H NMR). In addition, physicochemical properties such as thermal and electrochemical stabilities, ionic conductivity, and viscosity were evaluated. The NH_3 solubility in each IL was also measured at various pressures (1–5 bar) and temperatures (293.15–313.15 K) using a custom-made instrument, and the mole fraction of NH_3 was estimated using Peng-Robinson equation [11,17]. Further, the effects of the temperature, pressure, and functional groups of ILs on NH_3 solubility were elucidated.

2. Materials and methods

2.1. Materials

1-butylimidazole (98%, Sigma-Aldrich), 1-chloropentane (99%, Sigma-Aldrich), potassium trifluoromethanesulfonate (KOTf, Sigma-Aldrich), sodium tetrafluoroborate (NaBF₄, Sigma-Aldrich), benzyl chloride (99%, Sigma-Aldrich), dimethyl sulfoxide-D₆ (DMSO-d₆, 99.9%) + 0.05% V/V tetramethylsilane (TMS, Cambridge Isotope Laboratories, Inc.), NH_3 (99.99%), Ar gas (99.99%), and ethyl acetate (99.5%, Sigma-Aldrich) (Table 1) were used as received without any purification.

2.2. Instruments

The ionic conductivities and viscosities of the four different ILs were measured using a conductivity meter (CPC-401, Elmetron) and

Table 1

Materials for IL synthesis and characterization.

Materials	Molecular formula	CAS Number	Purity	Company
1-butylimidazole	C ₇ H ₁₂ N ₂	4316-42-1	98%	Sigma-Aldrich
1-chloropentane	C ₅ H ₁₁ Cl	543-59-9	99%	
Potassium trifluoromethanesulfonate	CF ₃ KO ₃ S	2926-27-4	98%	
Sodium tetrafluoroborate	NaBF ₄	13755-29-8	98%	
Ethyl acetate	C ₄ H ₈ O ₂	141-78-6	99.5%	
Dimethyl sulfoxide-D ₆ +0.05% V/V tetramethylsilane	C ₂ H ₆ OS + Si(CH ₃) ₄	2206-27-1	99.9%	Cambridge Isotope Laboratories, Inc.
Ammonia	NH ₃	–	99.9%	–
Argon	Ar	–	99.9%	–

a vibrating viscometer [SV-1A (0.3–1000 mPa·s), A&D company, limited], respectively. The FT-IR (4100, Jasco Inc.) and ^1H NMR (500 MHz, Bruker) spectrometers were used for IL structural analysis. The electrochemical windows of ILs were measured using a potentiostat (Autolab PGSTAT128 N Echochemie) controlled with the General Purpose Electrochemical System Software (version 4.9). In addition, an auto-thermogravimetric analyzer (Auto-TGA, Q500, TA instruments) and differential scanning calorimetry (DSC, Q2000, TA instruments) were used to evaluate the thermal properties of the ILs. NH_3 solubility capacity was measured using a self-made gas/liquid equilibrium instrument (Fig. S1 in the Electronic Supplementary Materials (ESM) that was modified from previous studies [11,17]. Further, a mass spectrometer (Q-Exactive Orbitrap mass spectrometer, Thermo Fisher Scientific) was used to validate the IL synthesis; each IL sample was diluted in LC/MS-grade methanol to a final concentration of $10\ \mu\text{M}$ and subsequently subjected to MS analysis. Electrospray was created with a spray voltage of 1.8 kV and a capillary temperature of $250\ ^\circ\text{C}$ while the solution was directly injected into a mass spectrometer with a flow rate of $5\ \mu\text{L}/\text{min}$ by automated syringe pump. The injected compounds were detected in a positive mode with a scan range of 150–2000 m/z . Data were collected for 3 min. After each analysis, the syringe and line used for sample injection were cleaned with ethanol to eliminate cross-contamination.

2.3. IL synthesis

The four ILs were synthesized through a metathesis reaction process comprising two key steps: (i) the formation of the desired cations and an exchangeable anion (e.g., $[\text{PBIM}]\text{Cl}$), and (ii) the reaction of the (i) with a suitable salt, incorporating the desired anion (e.g., NaBF_4). This process facilitates the synthesis of the desired IL (e.g., $[\text{PBIM}]\text{BF}_4$) with the intended cation and anion by exchanging the anion of the IL anion with that of the salt [23–25]. For example, $[\text{PBIM}]\text{BF}_4$ was synthesized using a modified protocol (Fig. 1) adopted from the literature [3,12]. 1-butylimidazole was first reacted with 1-chloropentane at a mole ratio of 1:1.1 in an oil bath at $60\ ^\circ\text{C}$ under vigorous stirring for 20 h. The synthesized $[\text{PBIM}]\text{Cl}$ was washed several times using ethyl acetate and then dried under vacuum at $70\ ^\circ\text{C}$ for 3 h. $[\text{PBIM}]\text{Cl}$ was then reacted for 10 h at $40\ ^\circ\text{C}$ with an equimolar amount of NaBF_4 . The obtained $[\text{PBIM}]\text{BF}_4$ was filtered and washed several times using ethyl acetate, followed by excess solvent removal at $90\ ^\circ\text{C}$ for 3 h under vacuum, yielding a yellowish product. $[\text{PBIM}]\text{OTf}$ was synthesized using the same method as $[\text{PBIM}]\text{BF}_4$, but the reaction time between $[\text{PBIM}]\text{Cl}$ and KOTf was 4 h. Further, $[\text{BzBIM}]\text{BF}_4$ was synthesized using the same method as $[\text{PBIM}]\text{BF}_4$ but benzyl chloride was added dropwise to 1-butylimidazole in the first step and the reaction mixture was stirred at $70\ ^\circ\text{C}$ for 20 h. The obtained yellowish product, $[\text{BzBIM}]\text{Cl}$, was washed with ethyl acetate several times to remove the unreacted reagents and then dried at $80\ ^\circ\text{C}$ for 3 h under vacuum. Subsequently, $[\text{BzBIM}]\text{Cl}$ was reacted with an equimolar amount of NaBF_4 for 10 h at $40\ ^\circ\text{C}$. The obtained $[\text{BzBIM}]\text{BF}_4$ was washed with distilled water to remove NaCl formed as a by-product. Finally, the excess solvent was evaporated at $70\ ^\circ\text{C}$ for 4 h, yielding a viscous, brownish product. $[\text{BzBIM}]\text{OTf}$ was synthesized using the same method as $[\text{BzBIM}]\text{BF}_4$, but the stirring time of the

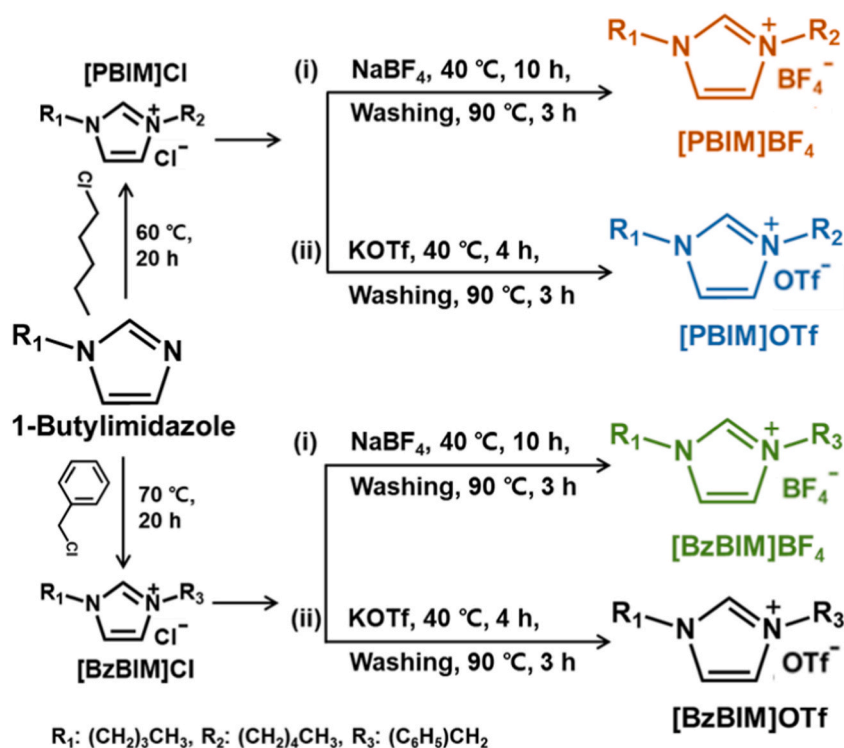


Fig. 1. Schematic of the stepwise synthesis of $[\text{PBIM}]\text{BF}_4$, $[\text{PBIM}]\text{OTf}$, $[\text{BzBIM}]\text{BF}_4$, and $[\text{BzBIM}]\text{OTf}$ ILs. (R_1 : butyl group; R_2 : pentyl group; and R_3 : benzyl group).

[BzBIM]Cl and KOTf reaction mixture was 4 h (Fig. 1). These steps were taken to ensure a comprehensive reaction between the reagents, ultimately yielding the desired product. Successful synthesis was confirmed through HR-MS, FT-IR, and ^1H NMR. The chemical shift assignments for ^1H NMR data of the four ILs are shown below.

[PBIM]BF₄: ^1H NMR (ppm, DMSO-*d*₆, 500 MHz), δ -ppm 8.41 (s, 1H, CH), 7.79–7.59 (dd, 2H, CH), 4.98–4.95 (t, 4H, CH₂), 4.67–4.64 (m, 4H, CH₂), 2.51–2.49 (t, 2H, CH₂), 2.35–2.32 (m, 2H, CH₂), 1.90–1.87 (m, 2H, CH₂), 1.55–1.47 (t, 6H, CH₃).

[PBIM]OTf: ^1H NMR (ppm, DMSO-*d*₆, 500 MHz), δ -ppm 8.17 (s, 1H, CH), 7.59 (s, 1H, CH), 7.47 (s, 1H, CH), 5.12–5.07 (t, 2H, CH₂), 4.75–4.72 (t, 2H, CH₂), 4.49–4.41 (m, 4H, CH₂), 2.34–2.32 (m, 2H, CH₂), 2.20–2.17 (m, 2H, CH₂), 1.77–1.74 (t, 2H, CH₂), 1.40–1.39 (t, 3H, CH₃), 1.38–1.35 (t, 3H, CH₃).

[BzBIM]BF₄: ^1H NMR (ppm, DMSO-*d*₆, 500 MHz), δ -ppm 9.73 (s, 1H, CH), 8.19 (s, 1H, CH), 8.17 (s, 1H, CH), 8.06 (s, 2H, Ar-H), 7.86–7.85 (t, 3H, Ar-H), 6.01 (s, 2H, CH₂), 4.72–4.69 (t, 2H, CH₂), 2.28–2.25 (3, 2H, CH₂), 1.73–1.69 (q, 2H, CH₂), 1.30–1.27 (t, 3H, CH₃).

[BzBIM]OTf: ^1H NMR (ppm, DMSO-*d*₆, 500 MHz), δ -ppm 9.92 (s, 1H, CH), 8.28 (s, 1H, CH), 8.24 (s, 1H, CH), 8.09–8.08 (t, 2H, Ar-H), 7.88–7.87 (t, 3H, Ar-H), 6.05 (s, 2H, CH₂), 4.75–4.72 (t, 2H, CH₂), 2.34–2.28 (m, 2H, CH₂), 1.79–1.73 (m, 2H, CH₂), 1.36–1.31 (t, 3H, CH₃).

2.4. Measurement of NH₃ solubility

The NH₃ solubility in the synthesized ILs was investigated using a gas/liquid equilibrium method. The NH₃ solubility in ILs was measured at temperature and pressure ranges of 293.15–323.15 K and 1–5 bar, respectively. The effect of different cations and anions in the ILs on NH₃ solubility was also investigated. The gas/liquid equilibrium setup used to determine the NH₃ solubility in the ILs is shown in Fig. S1. Initially, Ar gas was pumped through the solubility instrument at a mass flow rate of 200 standard cubic centimeters per minute (sccm) to investigate any leakage in the instrument pipelines. IL (30 mL) was placed in the absorption vessel, and a vacuum pump was used to remove all dissolved gases from the IL. The desired temperature was then set on a thermostat in a water bath. NH₃ gas was pumped from the storage tank to the absorption vessel at a mass flow rate of 200 sccm. The NH₃ gas was then directed to the absorption vessel at the desired pressure, and the liquid was mixed using a magnetic stirrer to increase the dissolution until equilibrium

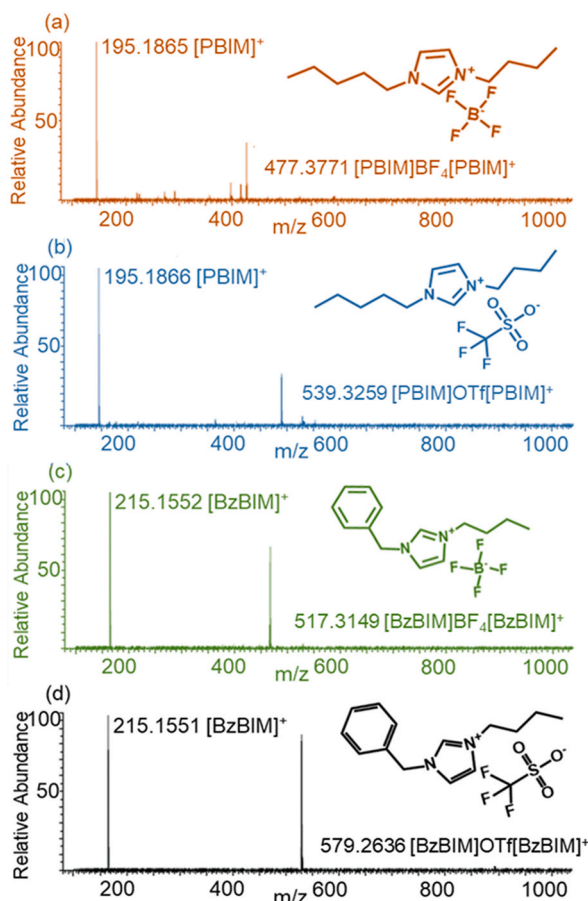


Fig. 2. Representative HR-MS spectra of (a) [PBIM]BF₄, (b) [PBIM]OTf, (c) [BzBIM]BF₄, and (d) [BzBIM]OTf.

was attained. Stirring was paused for approximately 5 min, during which no change in pressure was observed. Changes in pressure from 1 to 5 bar were recorded, and NH_3 solubility was calculated using Peng-Robinson equations (1) and (2), which are specifically developed for calculating gas-liquid equilibrium [11,17]:

$$P = \frac{RT}{V_m - b} - \frac{a}{V_m(V_m + b) + b(V_m - b)} \quad (1)$$

$$X_{\text{NH}_3} = \frac{n_{\text{NH}_3}}{n_{\text{NH}_3} + n_{\text{IL}}} \quad (2)$$

where P denotes the pressure, V_m denotes the molar volume, T denotes the temperature and R denotes the gas constant a and b are the cubic equation parameters, and n_{NH_3} , n_{IL} , and X_{NH_3} denote the amount of solubilized NH_3 , amount of IL, and mole fraction of solubilized NH_3 , respectively. Although these equations accurately represent the pressure-volume-temperature behavior of real gases and are applicable up to 7 bar, their accuracy in predicting solubility may diminish under pressures exceeding 7 bar [26].

2.5. Computational details

Semiempirical and density functional theory (DFT) calculations were performed to investigate the solvation mechanism of NH_3 in the ILs. The most favorable binding geometries of the IL [cation]anion, [cation]anion $\cdots\text{NH}_3$, and cation/anion $\cdots\text{NH}_3$ complexes (See Figs. S2 and S3 in ESM for the geometries) were obtained using an automated computational interaction site screening method implemented in the semiempirical XTb program [27,28]. The geometries were further refined at the B3LYP/6-31 + G* level of theory [29]. Frequency analyses were performed to obtain the solvation free energy, $\Delta G_{\text{solv}}^{\text{calc}}$, of NH_3 in the ILs at various temperatures and pressures. All DFT calculations were performed using the ORCA 5.0.3 program [30].

3. Results and discussion

3.1. Structural and physiochemical characterization of ILs

The four imidazolium-based ILs [PBIM]BF₄, [PBIM]OTf, [BzBIM]BF₄, and [BzBIM]OTf were synthesized by sharing the cations of [PBIM]⁺ and [BzBIM]⁺ and altering the anions as BF₄⁻ and OTf⁻ (Fig. 1). Their successful synthesis was confirmed by HR-MS. The average spectrum of each IL compound measured for 3 min is shown in Fig. 2. All compounds were highly pure and showed their corresponding positive imidazolium-based ions (i.e., [PBIM]⁺ and [BzBIM]⁺). For example, [PBIM]⁺ ions were recorded at 195.1865 m/z (a) and 195.1866 m/z (b), while [BzBIM]⁺ ions exhibited values in the range of 215.1551 m/z (c) to 215.1552 m/z (d). ILs with the corresponding imidazolium ions were also observed, indicating the presence of negative counter ions of IL ions. Also, [BF₄]⁻ and [OTf]⁻ were confirmed by the appearance of their complex forms; the m/z values of 477.3771 (a) and 517.3149 (c), along with 539.3259 (b) and 579.2636 (d), indicate the presence of the respective counter ions BF₄ and OTf in their corresponding IL complexes. The HR-MS analysis results conclusively affirm the successful synthesis of the ILs.

In addition, the IL synthesis was validated by the corresponding FT-IR peaks associated with the butyl chain and imidazolium ring in the cations, which are as follows: 2961 and 2870 cm⁻¹ corresponding to C–H stretching in CH₂ and CH₃, respectively, and 1641, 1508, 1463, and 752 cm⁻¹ ascribed to C=N stretching, aromatic C=C stretching, N–H stretching, and C–H bending, respectively, of the imidazolium ring structure (Fig. 3 and Table S1). The major differences between [PBIM]⁺ and [BzBIM]⁺ were the peaks associated with the pentyl and benzyl groups, respectively; 1379, 746, and 665 cm⁻¹ correspond to CH₃ bending, CH₂ rocking, and C–H bending,

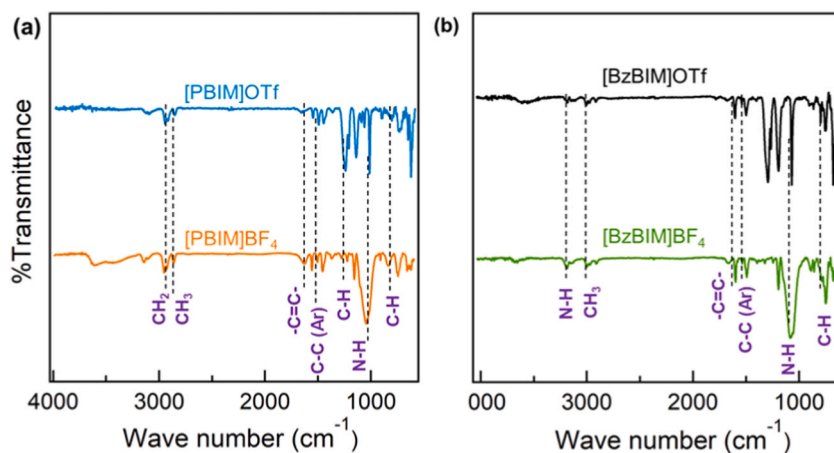


Fig. 3. Representative FT-IR spectra of (a) [PBIM]OTf and [PBIM]BF₄ and (b) [BzBIM]OTf and [BzBIM]BF₄.

respectively, confirming the presence of pentyl chains for $[\text{PBIM}]^+$, whereas 1498 and 708 cm^{-1} correspond to aromatic $\text{C}=\text{C}$ and $\text{C}-\text{H}$ bending, confirming the presence of the aromatic ring for $[\text{BzBIM}]^+$. More distinctively, when comparing the different anions for ILs with the same cation of $[\text{PBIM}]^+$, broad peaks at 1052 and 1151 cm^{-1} (Fig. 3a) characterized the presence of BF_4^- and OTf^- , respectively. Similar peaks were observed for BF_4^- and OTf^- with $[\text{BzBIM}]^+$ as the cation (Fig. 3b) [13,31].

The IL synthesis was further confirmed by assessing the chemical shift of ^1H NMR (Fig. 3). The $[\text{PBIM}]^+$ -based ILs (a) displayed a consistent chemical shift pattern because of the identical nature of the cations. Similarly, the $[\text{BzBIM}]^+$ -based ILs (b) exhibited comparable chemical shift trends. Nevertheless, the influence of BF_4^- and OTf^- impacted the cations, introducing slight variations in chemical shifts, particularly for the $[\text{PBIM}]^+$ -based ILs. BF_4^- , characterized by greater electronegativity and a smaller size than OTf^- , induced a shift toward the high-field region due to its stronger interaction with hydrogen atoms [32]. Conversely, the $[\text{BzBIM}]^+$ -based ILs exhibited minimal chemical shifts, attributable to the presence of a bulky benzyl ring attached to the imidazolium ring, which limits the mobility of hydrogen atoms and shields them from the influence of the surrounding environment (Fig. 4 and Table S2).

Thermal stability is a crucial factor when considering the use of ILs as electrolytes in various electrochemical applications, such as batteries, supercapacitors, and fuel cell membranes, where the electrochemical cell temperature may reach $220\text{ }^\circ\text{C}$ [33,34]. Thermal stability refers to the ability of a material to withstand high temperatures without significant decomposition or degradation. Several factors, such as the nature of the constituent cations and anions, symmetry, presence of functional groups, and overall chemical structure, affect the thermal stability of ILs [35]. Owing to their close interrelation with safety, durability, and chemical stability, the thermal stability of ILs plays a crucial role in electrochemical applications, such as electrosynthesis, electrocatalysis, and energy

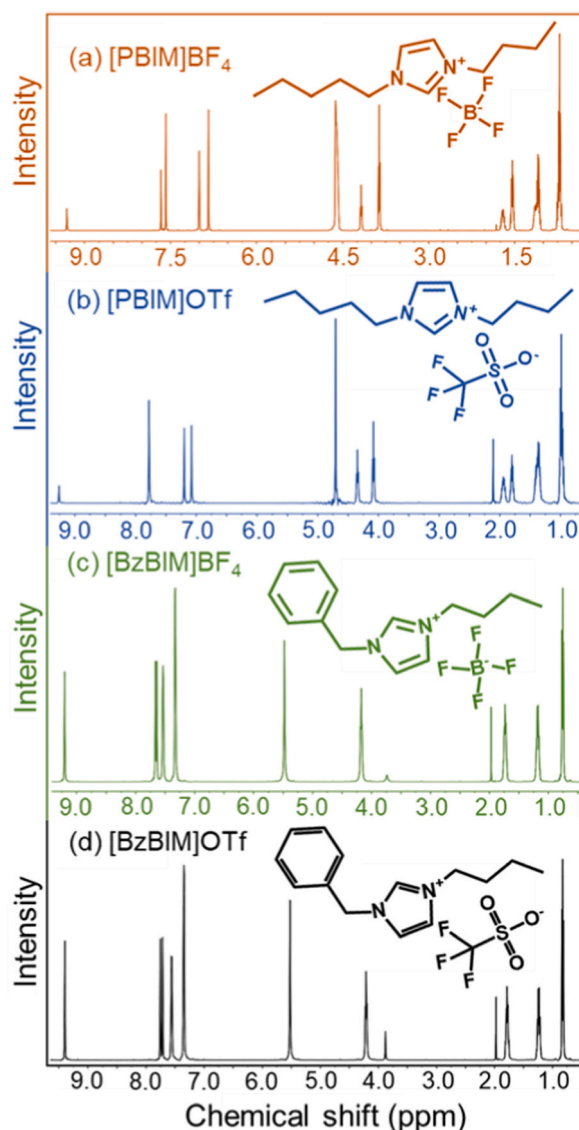


Fig. 4. Representative ^1H NMR spectra of (a) $[\text{PBIM}]\text{BF}_4$, (b) $[\text{PBIM}]\text{OTf}$, (c) $[\text{BzBIM}]\text{BF}_4$, and (d) $[\text{BzBIM}]\text{OTf}$.

storage [36]. Thus, the thermal stability of ILs is vital for ensuring the stability and performance of these applications under varying operational temperatures.

Thermogravimetric analysis of the synthesized ILs, performed in a temperature range of 25–500 °C, indicated that the [BzBIM]⁺-based ILs are more thermally stable than the [PBIM]⁺-based ILs. This is primarily due to the strong intermolecular π - π interaction of the benzyl group attached to the imidazolium ring (Fig. 5) [37]. Further, the [PBIM]⁺-based ILs exhibited lower thermal decomposition rates at 145 °C, attributable to the longer alkyl chains attached to the imidazolium ring. The presence of a longer chain increases van der Waals forces and weakens intramolecular electrostatic interactions. A longer chain also produces more stable carbocation and carbon radicals, thereby facilitating the decomposition reaction [38,39]. Moreover, the choice of anions in ILs affects their thermal stability depending on the coordinating nature, hydrophilicity, and nucleophilicity of the corresponding anion. BF₄⁻, characterized by higher coordinating ability, hydrophilicity, and nucleophilicity than OTf⁻, decreased the thermal stability of the ILs [38]. Thus, [PBIM]⁺ and [BzBIM]⁺ exhibited higher thermal stability when combined with OTf⁻ rather than BF₄⁻.

The phase behaviors, such as the melting temperature (T_m), glass transition temperature (T_g), and cold crystallization temperature (T_{cc}), of the ILs were measured using DSC. T_m and T_{cc} were measurable for [PBIM]⁺ but not for [BzBIM]⁺ because of the formation of amorphous glass and the lack of true phase transition behavior in [BzBIM]⁺ [40]. Such behavior can be attributed to the rigid and asymmetric structure of [BzBIM]⁺ due to the presence of the benzyl group, which has less flexibility than that of [PBIM]⁺, resulting in the lack of other transition behaviors while only having a T_g . The T_m values of the [PBIM]⁺-based ILs are relatively low regardless of the anion, indicating that they can be used as electrolytes for NH₃ electrolysis and storage, both of which are typically performed at low-temperatures (such as 25 °C) [41]. The T_m value of BF₄⁻ was slightly lower than that of OTf⁻ by ~1.5 °C, most likely due to the stronger interaction between the imidazolium cation and the smaller size of the anion [41,42]. The T_{cc} values of the [PBIM]⁺-based ILs showed considerably similar behavior, with partial crystallization at temperatures lower than T_m and temperatures higher than T_g [43]. BF₄⁻ exhibited a lower T_{cc} of ~5 °C than that of OTf⁻, most likely due to the long pentyl chain attached to the imidazolium ring, which provides a higher degree of freedom and symmetry [44,45] (Fig. 6). The T_g value indicates the temperature at which the transition from flexible to glassy state occurs [22]. The [PBIM]⁺-based ILs exhibited exceptionally low T_g values (-76.20 °C and -76.65 °C with BF₄⁻ and OTf⁻, respectively) compared with the [BzBIM]⁺-based ILs (-57.16 °C and -55.50 °C with BF₄⁻ and OTf⁻, respectively), most likely due to the flexibility of [PBIM]⁺. In addition, such low T_g values indicate that ions travel more easily through the liquid [46,47], resulting in enhanced ionic conductivity and decreased viscosity (Fig. 6). Thus, the [PBIM]⁺-based ILs are more promising for application as electrolytes even at low operating temperatures.

Ionic conductivity, viscosity, and electrochemical stability are important properties when considering the use of ILs as electrolytes in electrochemical applications. Ionic conductivity depends on the sizes of the constituent cationic and anionic species [48,49]. The ionic conductivity values of the four ILs measured at room temperature are listed in Table 2. The [PBIM]⁺-based ILs exhibited higher ionic conductivity than the [BzBIM]⁺-based ILs, attributable to the strong intermolecular π - π interaction facilitated by the presence of the benzyl group attached to the imidazolium ring, which may contribute to the lower ionic conductivity [37]. In addition, a larger anion size can reduce the ionic conductivity [48]. The smaller size of [PBIM]⁺ than [BzBIM]⁺ and the smaller size of BF₄⁻ than OTf⁻ contributed to the higher ionic conductivity of the [PBIM]⁺-based ILs.

Similar to ionic conductivity, viscosity is also affected by the size and structure of the cations and anions. However, it has an indirect relation with the ionic conductivity of ILs, affecting the moments of cations and anions; the higher the viscosity of the ILs, the lower the ionic conductivity, and vice versa. In the [PBIM]⁺- and [BzBIM]⁺-based ILs, anions have considerably little effect on viscosity, whereas cations have a considerable effect on viscosity. [PBIM]BF₄ and [PBIM]OTf had viscosities of 23.81 ± 2.41 and 25.70 ±

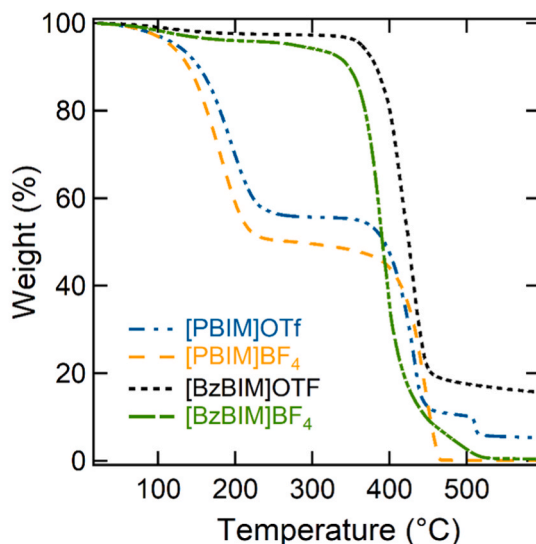


Fig. 5. Thermogravimetric analysis of ILs.

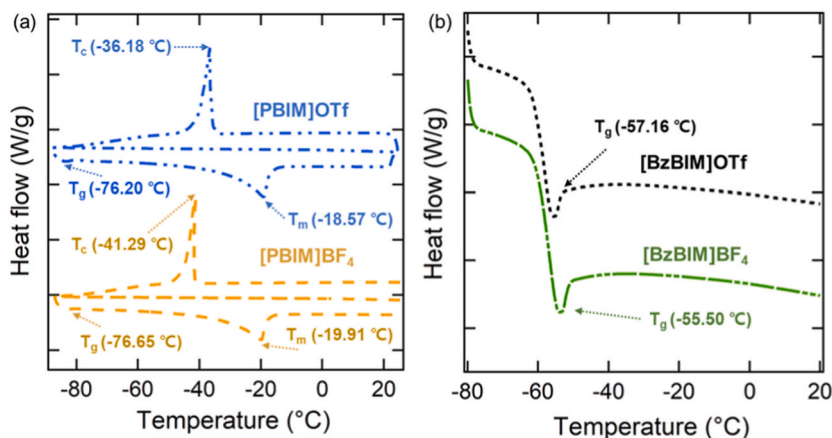


Fig. 6. Representative DSC spectra of (a) [PBIM]⁺-based ILs and (b) [BzBIM]⁺-based ILs.

Table 2

Viscosities, ionic conductivities, and potential windows of ILs at room temperature under atmospheric pressure.

Ionic liquid	Conductivity (mS/cm)	Viscosity (mPa·s)	Potential window (V)
[PBIM]BF ₄	4.23 ± 0.27	23.81 ± 2.41	2.96
[PBIM]OTf	2.75 ± 0.39	25.70 ± 2.52	2.48
[BzBIM]BF ₄	0.60 ± 0.08	363.02 ± 4.51	2.78
[BzBIM]OTf	0.80 ± 0.17	358.01 ± 2.11	2.25

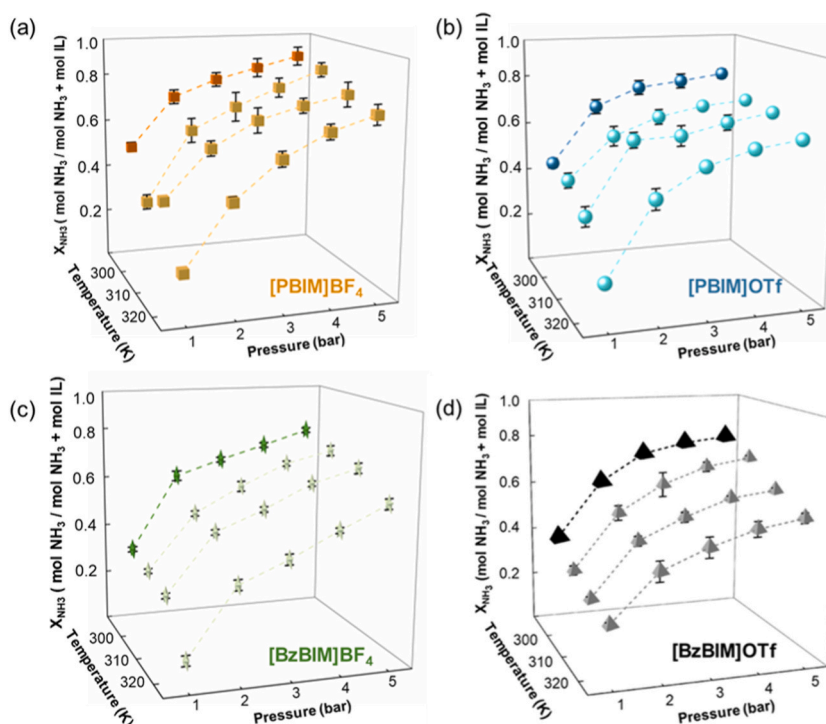


Fig. 7. NH₃ solubility in (a) [PBIM]BF₄, (b) [PBIM]OTf, (c) [BzBIM]BF₄, and (d) [BzBIM]OTf at various temperatures and pressures. Each IL's NH₃ solubility at 293.15 K with changing pressure is indicated by a darker marker and a thicker line.

2.52 mPa·s, respectively, while [BzBIM]BF₄ and [BzBIM]OTf had higher viscosity values of 363.02 ± 4.51 and 358.01 ± 2.11 mPa·s, respectively (Table 2). Such an increase in viscosity is mainly due to the higher charge density of the [BzBIM]⁺-based ILs, which enhances electrostatic interactions and strengthens the intensity of intermolecular interactions [50,51].

Electrochemical stability, which determines the feasible range of operating voltages [52,53], was investigated using cyclic voltammetry (CV) via a three-electrode configuration, with a Ni mesh as the working electrode, Ag/AgCl as the reference electrode, and graphite as the counter electrode. The working electrode was chosen as Ni mesh because of its use in NH₃ electrolysis [54,55]. Representative CV data with the potential window range are shown in Fig. S4 and Table 2. The [BzBIM]⁺-based ILs showed lower electrochemical potential windows than the [PBIM]⁺-based ILs, attributable to the presence of an aromatic ring with vacant π^* orbitals [52]. The increase in the length of the alkyl chains attached to the imidazolium ring increases the LUMO energy, ultimately increasing the electrochemical potential window of the corresponding IL [56]. In addition, the smaller size of BF₄⁻ than OTf⁻ contributed to a larger HOMO-LUMO gap, resulting in higher electrochemical stability [56]. [PBIM]BF₄ and [PBIM]OTf exhibited electrochemical potential window values of 2.96 and 2.48 V, respectively, and [BzBIM]BF₄ and [BzBIM]OTf showed electrochemical potential window values of 2.78 and 2.25 V, respectively.

3.2. NH₃ solubility in ILs

3.2.1. Temperature and pressure dependence

NH₃ solubility in the synthesized ILs was investigated at different pressures and temperatures, where their solubility characteristics critically rely on three parameters [57]: (i) a free volume resulting from the interaction of different cation and anion structures in ILs before NH₃ adsorption, (ii) an increase in the volume of NH₃-ILs due to NH₃ adsorption onto ILs, and (iii) IL viscosity. The equilibria of these three parameters have a combined effect on solubility. As shown in Fig. 7, the overall NH₃ solubility decreases with increasing temperature but increases with increasing pressure, as reported in previous studies [11,58]. For example, the fractional solubility (mol NH₃/mol NH₃ + mol IL) in the [PBIM]⁺-based ILs (Fig. 7 a, b) was generally higher than that of the [BzBIM]⁺-based ILs (Fig. 7 c, d) at pressures of 1–5 bars and a fixed temperature of 293.15 K (Table S3) due to the higher viscosity of [BzBIM]⁺ than [PBIM]⁺, thereby impeding NH₃ adsorption on the IL and anion-cation interaction and hence lowering solubility. A very similar trend was observed at temperatures of 303.15–323.15 K. Our findings are consistent with those of a previous study on [C₄MIM]BF₄-based ILs, which showed that the fractional NH₃ solubility ranges from 0.2153 to 0.6291 at 293.15 K and pressures of 1.4–5.5 bars [18]. The influence of IL cations and anions on NH₃ solubility will be further discussed at a fixed temperature but varying pressure.

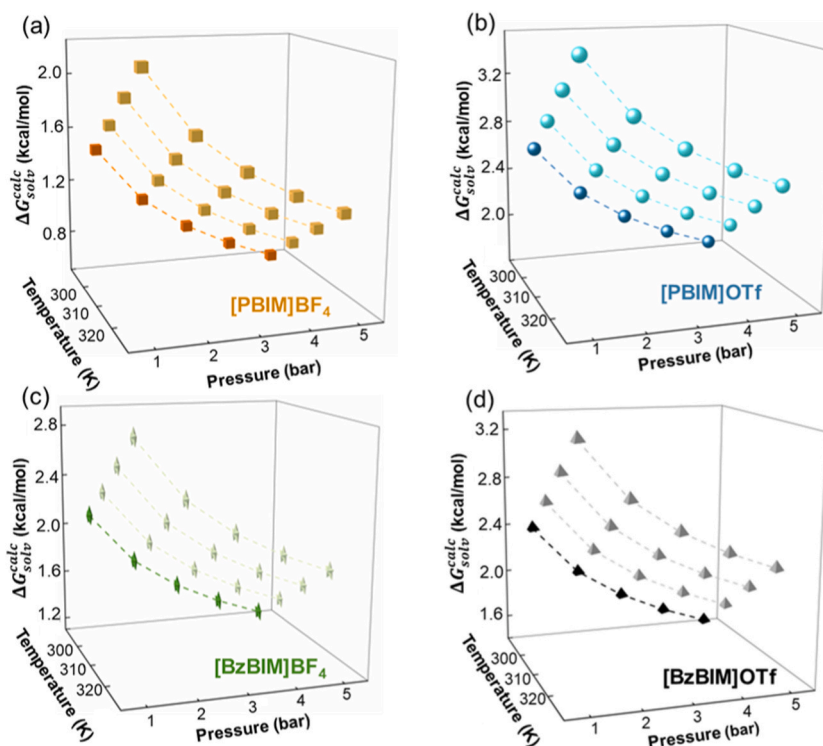


Fig. 8. Solvation free energy (ΔG_{solv}^{calc}) of NH₃ in (a) [PBIM]BF₄, (b) [PBIM]OTf, (c) [BzBIM]BF₄, and (d) [BzBIM]OTf at various temperatures (293.15, 303.15, 313.15, and 323.15 K) and pressures (1, 2, 3, 4, and 5 bar).

3.2.2. Simulation of the solvation free energy ($\Delta G_{\text{sol}}^{\text{calc}}$) of NH_3 in ILs

DFT calculations were used to substantiate the experimental results of NH_3 solubility in ILs. Theoretically, a lower solvation free energy ($\Delta G_{\text{sol}}^{\text{calc}}$) corresponds to higher NH_3 solubility. As shown in Fig. 8, at a fixed temperature, the calculated $\Delta G_{\text{sol}}^{\text{calc}}$ decreases with increasing pressure for all studied temperature conditions, indicating enhanced solubility at higher pressures (Table S5 for $\Delta G_{\text{sol}}^{\text{calc}}$ values). Conversely, as the temperature increases, the calculated $\Delta G_{\text{sol}}^{\text{calc}}$ increases, resulting in diminished solubility at elevated temperatures. Overall, the pressure- and temperature-dependence of the calculated $\Delta G_{\text{sol}}^{\text{calc}}$ agreed well with the experimental observations for all four ILs. Further, the relationship between NH_3 solubility in ILs and the calculated $\Delta G_{\text{sol}}^{\text{calc}}$ at 293.15 K and 5 bar in Fig. 9 clearly revealed that [PBIM]BF₄ exhibited superior solubility among the ILs and the smaller the calculated $\Delta G_{\text{sol}}^{\text{calc}}$, the greater NH_3 solubility. This trend remains consistent across all examined temperatures and pressures. The superior solubility of [PBIM]BF₄ can be ascribed to the minimal reorganization of the [cation]anion complex structure upon NH_3 solvation (Fig. S2 in ESM). This suggests that [PBIM]BF₄ forms a hydrogen bonding with the NH_3 solute while keeping the cation-anion interaction almost intact (see Fig. 9).

3.2.3. Effects of cations and anions

The characteristics of the cations or anions of ILs, such as size and charge interaction strength, in addition to the viscosity properties, can affect the NH_3 solubility in ILs. As briefly mentioned in Section 3.2.1, the [BzBIM]⁺-based ILs showed a lower solubility mole fraction of NH_3 than the [PBIM]⁺-based ILs, regardless of the anion, at temperatures ranging from 293.15 to 323.15 K and pressures ranging from 1 to 5 bar. For example, the solubility mole fractions for [BzBIM]BF₄ and [BzBIM]OTf were 0.773 ± 0.010 and 0.776 ± 0.020 mol NH_3 /mol $\text{NH}_3 + \text{mol IL}$, respectively, compared with 0.861 ± 0.041 and 0.790 ± 0.016 mol NH_3 /mol $\text{NH}_3 + \text{mol IL}$ for [PBIM]BF₄ and [PBIM]OTf, respectively, at 293.15 K and 5 bar (see the darker markers and thicker lines in Fig. 7 a-d). Such low solubility capacities of the [BzBIM]⁺-based ILs can be explained by their smaller size due to the presence of the shorter length of the alkyl side chain attached to the imidazolium ring than that of the [PBIM]⁺-based ILs, resulting in enhanced electrostatic interaction but reduced free volume of the IL cation and anion components [59,60].

The DFT calculation also validated the enhanced electrostatic interaction in the BzBIM⁺... NH_3 complex with a lower binding free energy [ΔG_{bind} (BzBIM⁺... NH_3) = -1.92 kcal/mol at 293.15 K and 1 atm] than that in the PBIM⁺... NH_3 complex [ΔG_{bind} (PBIM⁺... NH_3) = -1.80 kcal/mol at 293.15 K and 1 atm] (Fig. S3 in ESM). As a result, the adsorption of NH_3 onto ILs will be reduced, as will the volume of NH_3 -ILs. In addition, the relatively higher viscosity of the [BzBIM]⁺-based ILs, due to a butyl alkyl chain on one side and a benzyl group on the other side of the imidazolium ring, can decrease the NH_3 transfer rate during the dissolution process. The combination of the above-described factors will overall cause reduced NH_3 solubility in the [BzBIM]⁺ [59,61].

For the anions of the ILs, OTf⁻ and BF₄⁻, which are both fluorinated, were chosen to increase NH_3 solubility via hydrogen bonding with hydrogen atoms in NH_3 [62]. NH_3 has three hydrogen bonding donors, whereas OTf⁻ and BF₄⁻ have six and four acceptors, respectively, facilitating the formation of robust hydrogen bonds between these anions and the hydrogen atoms of NH_3 [17]. When comparing BF₄⁻ and OTf⁻ with the same cation of [PBIM]⁺ in ILs, OTf⁻ demonstrated inferior NH_3 solubility capacity at 293.15 K than BF₄⁻. This might be because the OTf⁻ size was substantially larger than the BF₄⁻ size, resulting in a higher molar density and lower free volume, which in turn led to less space available for NH_3 to occupy and hence decreased solubility [63]. The DFT calculation further revealed that the interaction between NH_3 and BF₄⁻ [ΔG_{bind} (BF₄⁻... NH_3) = 3.28 kcal/mol at 293.15 K and 1 atm] is more favorable than that between NH_3 and OTf⁻ [ΔG_{bind} (OTf⁻... NH_3) = 4.81 kcal/mol at 293.15 K and 1 atm] (Fig. S3). However, the opposite result was observed for [BzBIM]⁺ with BF₄⁻ and OTf⁻. This indicates that not only the anion and cation size but also the viscosity nature of ILs can more critically affect the NH_3 solubility behavior. Because the viscosity of [BzBIM]OTf is lower than that of [BzBIM]BF₄, although the OTf⁻ size is larger than the BF₄⁻ size, the NH_3 solubility in [BzBIM]OTf was higher than that in [BzBIM]BF₄ at all temperatures (Fig. 7 c, d thicker lines).

In summary, the NH_3 solubility in the four synthesized ILs was either similar or slightly superior to that of previously reported ILs with different cations and anions (Table S4). For instance, NH_3 solubility at 293.15 K and 5.5 bar in the ILs with the BF₄⁻ anion (the same as in the current work) but with the cation having different alkyl chains on either side of the imidazolium ring, such as [C₂MIM]⁺, [C₄MIM]⁺, and [C₆MIM]⁺, was 1.22 and 1.06 times lower than those in [PBIM]⁺ and [BzBIM]⁺, respectively [18]. Similarly, ILs containing BF₄⁻ and a cation with a hydroxyl functional group on one side of the imidazolium ring, including [EtOHmim]⁺, exhibited lower solubility capacities for NH_3 than [PBIM]⁺ and [BzBIM]⁺ [17]. By contrast, [EtOHmim]PF₆ exhibited a higher NH_3 solubility capacity than [EtOHmim]BF₄ at a 4.74 bar [9,17].

4. Conclusions

The successful synthesis of four imidazolium-based ILs namely, [PBIM]OTf, [PBIM]BF₄, [BzBIM]OTf, and [BzBIM]BF₄, was confirmed using FT-IR, HR-MS, and ¹H NMR. All synthesized ILs were stable in the temperature range of 145 °C and 450 °C and exhibited extraordinarily wide electrochemical potential windows (within 2.25–2.96 V). In addition, all ILs exhibited superb NH_3 solubility capacity because of the long alkyl chains and benzyl groups attached to either side of the imidazolium ring and the presence of fluorinated anions, which are considered to be the key factors contributing to the high NH_3 solubility in these ILs. Notably, the [PBIM]⁺-based ILs [PBIM]OTf and [PBIM]BF₄ exhibited higher NH_3 solubility than the [BzBIM]⁺-based ILs [BzBIM]OTf and [BzBIM]BF₄. Among the four ILs, [PBIM]BF₄ exhibited the highest NH_3 solubility (0.861 ± 0.041 mol NH_3 /mol $\text{NH}_3 + \text{mol IL}$, at 293.15 K and 5 bar) because of its lowest viscosity and longest alkyl chains. Notably, solubility measurements at temperatures and pressures higher than those explored in this study may yield more accurate predictions through the application of alternative models and computational

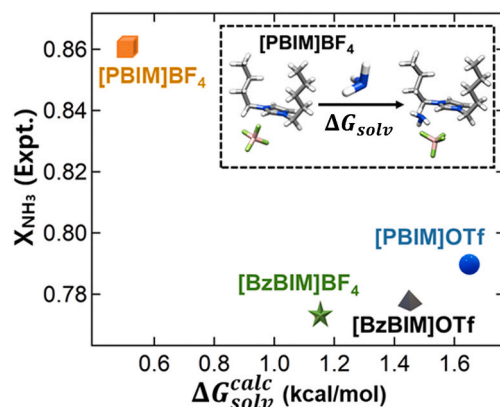


Fig. 9. Comparison of experimental solubility results with simulation results (ΔG_{solv}^{calc}) at 293.15 K and 5 bar for the four ILs.

procedures. Future directions could involve leveraging tools such as the statistical associating fluid theory and universal quasichemical activity coefficient for higher precision [64,65]. Overall, it can be concluded that the NH_3 solubility characteristics in the four ILs are largely dependent on the viscosities and cation and anion structures of ILs, which either enhance the free volume or impedes NH_3 the transportation and adsorption. Owing to their promising NH_3 solubility behavior, these ILs will have significant applications in NH_3 storage and electrolysis.

Data availability statement

Data will be made available on request.

CRediT authorship contribution statement

Muhammad Salman: Writing – original draft, Investigation, Formal analysis, Data curation. **Ji Won Lee:** Writing – review & editing, Investigation, Formal analysis. **Sang Hyuk Lee:** Writing – review & editing, Validation, Methodology. **Min Ho Lee:** Writing – review & editing, Data curation. **Van Duc Pham:** Writing – review & editing, Data curation. **Min-Sik Kim:** Writing – review & editing, Validation, Methodology. **Daeheum Cho:** Writing – review & editing, Validation, Methodology, Data curation. **Hye Jin Lee:** Writing – review & editing, Supervision, Conceptualization.

Declaration of competing interest

The authors declare the following financial interests/personal relationships which may be considered as potential competing interests: Hye Jin Lee, Muhammad Salman, Ji Won Lee, and Sang Hyuk Lee have patent #10-2022-0166635 pending to Assignee: Korea Electric Power Corporation and Kyungpook National University Industry-Academic Cooperation Foundation. If there are other authors, they declare that they have no known competing financial interests or personal relationships that could have appeared to influence the work reported in this paper.

Acknowledgements

This research was supported by the Korea Electric Power Corporation (Grant number: R20X002-24) and the National Research Foundation of Korea (NRF) grant, funded by the Korean government (Ministry of Science and ICT, MSIT) (Grant number: RS-2023-00207831) to Prof. H. J. L.; NRF-2022R1A2C2013377 to Prof. M.-S. K.

Appendix A. Supplementary data

Supplementary data to this article can be found online at <https://doi.org/10.1016/j.heliyon.2024.e24305>.

References

- [1] Y. Chaker, H. Ilikti, M. Debdab, T. Moumene, E.H. Belarbi, A. Wadouachi, O. Abbas, B. Khelifa, S. Bresson, Synthesis and characterization of 1-(hydroxyethyl)-3-methylimidazolium sulfate and chloride ionic liquids, *J. Mol. Struct.* 1113 (2016) 182–190, <https://doi.org/10.1016/j.molstruc.2016.02.017>.
- [2] I. Short, A. Sahgal, W. Hayduk, Solubility of ammonia and hydrogen sulfide in several polar solvents, *J. Chem. Eng. Data* 28 (1983) 63–66, <https://doi.org/10.1021/je00031a019>.

- [3] S.A. Dharaskar, K.L. Wasewar, M.N. Varma, D.Z. Shende, C.K. Yoo, Synthesis, characterization and application of 1-butyl-3-methylimidazolium tetrafluoroborate for extractive desulfurization of liquid fuel, *Arab. J. Chem.* 9 (2016) 578–587, <https://doi.org/10.1016/j.arabjc.2013.09.034>.
- [4] S.E. Sanni, D.A. Vershima, E.E. Okoro, B.A. Oni, Technological advancements in the use of ionic liquid-membrane systems for CO₂ capture from biogas/flue gas - a review, *Heliyon* 8 (2022) e12233, <https://doi.org/10.1016/j.heliyon.2022.e12233>.
- [5] P.F. Arce, P.A. Robles, T.A. Graber, M. Aznar, Modeling of high-pressure vapor-liquid equilibrium in ionic liquids + gas systems using the PRSV equation of state, *Fluid Phase Equil.* 295 (2010) 9–16, <https://doi.org/10.1016/j.fluid.2010.03.030>.
- [6] Q.F. Wang, L.J. Liang, J.B. Sun, J. Zhou, Application of a reversed-phase ionic liquid dispersive liquid-liquid microextraction method for the extraction and preconcentration of domoic acid from urine samples, *Heliyon* 8 (2022) e10152, <https://doi.org/10.1016/j.heliyon.2022.e10152>.
- [7] E.A. Moneer, B.A. Bakr, S.H. Akl, Y.H. Shahin, B.H. Elwakil, M. Hagar, K.R. Paudel, A. Aljuhani, M.R. Aouad, N. Rezki, Design and synthesis of novel bis-pyridinium based-ionic liquids as potent antiparasitic agents, *Heliyon* 9 (2023) e15431, <https://doi.org/10.1016/j.heliyon.2023.e15431>.
- [8] L. Zhang, H. Dong, S. Zeng, Z. Hu, S. Hussain, X. Zhang, An overview of ammonia separation by ionic liquids, *Ind. Eng. Chem. Res.* 60 (2021) 6908–6924, <https://doi.org/10.1021/acs.iecr.1c00780>.
- [9] A. Yokozeki, M.B. Shiflett, Ammonia solubilities in room-temperature ionic liquids, *Ind. Eng. Chem. Res.* 46 (2007) 1605–1610, <https://doi.org/10.1021/ie061260d>.
- [10] Y.T. Hsieh, T. Tsuda, S. Kuwabata, SEM as a facile tool for real-time monitoring of microcrystal growth during electrodeposition: the merit of ionic liquids, *Anal. Chem.* 89 (2017) 7249–7254, <https://doi.org/10.1021/acs.analchem.7b01596>.
- [11] L. Yuan, H. Gao, H. Jiang, S. Zeng, T. Li, B. Ren, X. Zhang, Experimental and thermodynamic analysis of NH₃ absorption in dual-functionalized pyridinium-based ionic liquids, *J. Mol. Liq.* 323 (2021) 114601, <https://doi.org/10.1016/j.molliq.2020.114601>.
- [12] S. Han, M. Luo, X. Zhou, Z. He, L. Xiong, Synthesis of dipentyl carbonate by transesterification using basic ionic liquid [bmim]OH catalyst, *Ind. Eng. Chem. Res.* 51 (2012) 5433–5437, <https://doi.org/10.1021/ie202628m>.
- [13] G. Lakshminarayana, M. Nogami, Proton conducting organic-inorganic composite membranes under anhydrous conditions synthesized from tetraethoxysilane/methyltriethoxysilane/trimethyl phosphate and 1-butyl-3-methylimidazolium tetrafluoroborate, *Solid State Ionics* 181 (2010) 760–766, <https://doi.org/10.1016/j.ssi.2010.03.035>.
- [14] A. Yokozeki, M.B. Shiflett, Ammonia solubilities in room-temperature ionic liquids, *Ind. Eng. Chem. Res.* 46 (2007) 1605–1610, <https://doi.org/10.1021/ie061260d>.
- [15] T. Wasilewski, J. Gębicki, W. Kamysz, Prospects of ionic liquids application in electronic and bioelectronic nose instruments, *TRAC Trends Anal. Chem.* (Reference Ed.) 93 (2017) 23–36, <https://doi.org/10.1016/j.trac.2017.05.010>.
- [16] J. Flieger, M. Flieger, Ionic liquids toxicity-benefits and threats, *Int. J. Mol. Sci.* 21 (17) (2020) 6267, <https://doi.org/10.3390/ijms21176267>.
- [17] Z. Li, X. Zhang, H. Dong, X. Zhang, H. Gao, S. Zhang, J. Li, C. Wang, Efficient absorption of ammonia with hydroxyl-functionalized ionic liquids, *RSC Adv.* 5 (2015) 81362–81370, <https://doi.org/10.1039/c5ra13730f>.
- [18] G. Li, Q. Zhou, X. Zhang, LeiWang, S. Zhang, J. Li, Solubilities of ammonia in basic imidazolium ionic liquids, *Fluid Phase Equil.* 297 (2010) 34–39, <https://doi.org/10.1016/j.fluid.2010.06.005>.
- [19] Z. Zhu, W. Bai, Y. Xu, H. Gong, Y. Wang, D. Xu, J. Gao, Liquid-liquid extraction of methanol from its mixtures with hexane using three imidazolium-based ionic liquids, *J. Chem. Thermodyn.* 138 (2019) 189–195, <https://doi.org/10.1016/j.jct.2019.06.024>.
- [20] J. Gao, Y. Ma, L. Zhang, W. Liu, D. Xu, X. Xu, Y. Wang, Measurement and correlation of phase equilibria for ternary systems of water + (ethanol/1-propanol) + 1-decyl-3-methylimidazolium bis(trifluoromethylsulfonyl) imide at 298.15 K, *Fluid Phase Equil.* 427 (2016) 340–344, <https://doi.org/10.1016/j.fluid.2016.07.024>.
- [21] C.P. Fredlake, J.M. Crosthwaite, D.G. Hert, S.N.V.K. Aki, J.F. Brennecke, Thermophysical properties of imidazolium-based ionic liquids, *J. Chem. Eng. Data* 49 (2004) 954–964, <https://doi.org/10.1021/je0034261a>.
- [22] A. Shrivastava, Introduction to Plastics Engineering, William Andrew, 2018, <https://doi.org/10.1016/b978-0-323-39500-7.00001-0>.
- [23] K. Li, H.M. Titi, P. Berton, R.D. Rogers, Porphyrinic ionic liquid dyes: synthesis and characterization, *ChemistryOpen* 7 (2018) 659–663, <https://doi.org/10.1002/open.201800166>.
- [24] S.K. Singh, A.W. Savoy, Ionic liquids synthesis and applications: an overview, *J. Mol. Liq.* 297 (2020) 112038, <https://doi.org/10.1016/j.molliq.2019.112038>.
- [25] M. Javaherian, S.J. Saghanehzad, Synthesis, characterization and applications of dicationic ionic liquids in organic synthesis, *Mini Rev. Org. Chem.* 17 (2020) 450–464, <https://doi.org/10.2174/1570193X16666190508091231>.
- [26] A.K. Biñ, Prediction of oxygen and ozone solubility in liquids with the peng-robinson equation of state, *Ozone Sci. Eng.* 30 (2008) 13–20, <https://doi.org/10.1080/01919510701728384>.
- [27] C. Bannwarth, S. Ehlert, S. Grimme, GFN2-xTB-An accurate and broadly parametrized self-consistent tight-binding quantum chemical method with multipole electrostatics and density-dependent dispersion contributions, *J. Chem. Theor. Comput.* 15 (2019) 1652–1671, <https://doi.org/10.1021/acs.jctc.8b01176>.
- [28] C. Plett, S. Grimme, Automated and efficient generation of general molecular aggregate structures, *Angew. Chem. Int. Ed. Engl.* 62 (2023) e202214477, <https://doi.org/10.1002/anie.202214477>.
- [29] A.D. Becke, A new mixing of Hartree-Fock and local density-functional theories, *J. Chem. Phys.* 98 (1993) 1372–1377, <https://doi.org/10.1063/1.464304>.
- [30] F. Neese, Software update: the ORCA program system—version 5.0, *Wiley Interdiscip. Rev. Comput. Mol. Sci.* 12 (2022) e1606, <https://doi.org/10.1002/wcms.1606>.
- [31] Z. Zhou, G. Huang, Y. Xiong, M. Zhou, S. Zhang, C.Y. Tang, F. Meng, Unveiling the susceptibility of functional groups of poly(ether sulfone)/polyvinylpyrrolidone membranes to NaOCl: a two-dimensional correlation spectroscopic study, *Environ. Sci. Technol.* 51 (2017) 14342–14351, <https://doi.org/10.1021/acs.est.7b03952>.
- [32] H.V. Huynh, T.T. Lam, H.T.T. Luong, Anion influences on reactivity and NMR spectroscopic features of NHC precursors, *RSC Adv.* 8 (2018) 34960–34966, <https://doi.org/10.1039/c8ra05839c>.
- [33] D. Muñoz-Rojas, J.-B. Leriche, C. Delacourt, P. Poizot, M.R. Palacín, J.-M. Tarascon, Development and implementation of a high temperature electrochemical cell for lithium batteries, *Electrochem. Commun.* 9 (2007) 708–712, <https://doi.org/10.1016/j.elecom.2006.11.005>.
- [34] L.W. Le Fevre, A. Ejigu, R. Todd, A.J. Forsyth, R.A.W. Dryfe, High temperature supercapacitors using water-in-salt electrolytes: stability above 100 °C, *Chem. Commun.* 57 (2021) 5294–5297, <https://doi.org/10.1039/d1cc01087e>.
- [35] Y. Chen, X. Han, Z. Liu, Y. Li, H. Sun, H. Wang, J. Wang, Thermal decomposition and volatility of ionic liquids: factors, evaluation and strategies, *J. Mol. Liq.* 366 (2022) 120336, <https://doi.org/10.1016/j.molliq.2022.120336>.
- [36] H. Liu, H. Yu, Ionic liquids for electrochemical energy storage devices applications, *J. mater. sci. technol.* 35 (2019) 674–686, <https://doi.org/10.1016/j.jmst.2018.10.007>.
- [37] M. Kermaniaryani, M.I.A. Mutalib, Y. Dong, K.C. Lethesh, O.B.O. Ben Ghanem, K.A. Kurnia, N.F. Aminuddin, J.-M. Leveque, Physicochemical properties of new imidazolium-based ionic liquids containing aromatic group, *J. Chem. Eng. Data* 61 (2016) 2020–2026, <https://doi.org/10.1021/acs.jced.5b00983>.
- [38] C. Maton, N. De Vos, C.V. Stevens, Ionic liquid thermal stabilities: decomposition mechanisms and analysis tools, *Chem. Soc. Rev.* 42 (2013) 5963–5977, <https://doi.org/10.1039/c3cs60071h>.
- [39] Y. Cao, T. Mu, Comprehensive investigation on the thermal stability of 66 ionic liquids by thermogravimetric analysis, *Ind. Eng. Chem. Res.* 53 (2014) 8651–8664, <https://doi.org/10.1021/ie5009597>.
- [40] E. Gómez, N. Calvar, Á. Domínguez, Thermal Behaviour of Pure Ionic Liquids, *Ionic Liquids - Current State of the Art*, 2015, p. 199, <https://doi.org/10.5772/59271>.
- [41] T. Poppel, C. Roth, K. Fumino, D. Paschek, M. Kockerling, R. Ludwig, The influence of hydrogen-bond defects on the properties of ionic liquids, *Angew. Chem. Int. Ed.* 50 (2011) 6661–6665, <https://doi.org/10.1002/ange.201100199>.
- [42] J.M. Pringle, J. Golding, K. Baranyai, C.M. Forsyth, G.B. Deacon, J.L. Scott, D.R. MacFarlane, The effect of anion fluorination in ionic liquids—physical properties of a range of bis(methanesulfonyl)amide salts, *New J. Chem.* 27 (2003) 1504–1510, <https://doi.org/10.1039/b304072k>.

- [43] K. Ishino, H. Shingai, Y. Hikita, I. Yoshikawa, H. Houjou, K. Iwase, Cold crystallization and the molecular structure of imidazolium-based ionic liquid crystals with a p-nitroazobenzene moiety, *ACS Omega* 6 (2021) 32869–32878, <https://doi.org/10.1021/acsomega.1c04866>.
- [44] H.L. Ngo, K. LeCompte, L. Hargens, A.B. McEwen, Thermal properties of imidazolium ionic liquids, *Thermochim. Acta* 357–358 (2000) 97–102, [https://doi.org/10.1016/s0040-6031\(00\)00373-7](https://doi.org/10.1016/s0040-6031(00)00373-7).
- [45] C.P. Fredlake, J.M. Crosthwaite, D.G. Hert, S.N.V.K. Aki, J.F. Brennecke, Thermophysical properties of imidazolium-based ionic liquids, *J. Chem. Eng. Data* 49 (2004) 954–964, <https://doi.org/10.1021/je034261a>.
- [46] H. Hu, W. Yuan, L. Lu, H. Zhao, Z. Jia, G.L. Baker, Low glass transition temperature polymer electrolyte prepared from ionic liquid grafted polyethylene oxide, *J. Polym. Sci., Part A: Polym. Chem.* 52 (2014) 2104–2110, <https://doi.org/10.1002/pola.27217>.
- [47] F. Zhang, Y. Sun, Z. Wang, D. Fu, J. Li, J. Hu, J. Xu, X. Wu, Highly conductive polymeric ionic liquid electrolytes for ambient-temperature solid-state lithium batteries, *ACS Appl. Mater. Interfaces* 12 (2020) 23774–23780, <https://doi.org/10.1021/acsami.9b22945>.
- [48] W.L. Yuan, X. Yang, L. He, Y. Xue, S. Qin, G.H. Tao, Viscosity, conductivity, and electrochemical property of dicyanamide ionic liquids, *Front. Chem.* 6 (2018) 59, <https://doi.org/10.3389/fchem.2018.00059>.
- [49] W.J. Li, B.X. Han, R.T. Tao, Z.F. Zhang, J.L. Zhang, Measurement and correlation of the ionic conductivity of ionic liquid-molecular solvent solutions, *Chin. J. Chem.* 25 (2007) 1349–1356, <https://doi.org/10.1002/cjoc.200790251>.
- [50] R. Tao, S.L. Simon, Rheology of imidazolium-based ionic liquids with aromatic functionality, *J. Phys. Chem. B* 119 (2015) 11953–11959, <https://doi.org/10.1021/acs.jpcc.5b06163>.
- [51] J.E. Bara, A. Finotello, J.W. Magee, S. Qian, K.E. O’Harra, G.P. Dennis, R.D. Noble, 110th anniversary: properties of imidazolium-based ionic liquids bearing both benzylic and n-alkyl substituents, *Ind. Eng. Chem. Res.* 58 (2019) 17956–17964, <https://doi.org/10.1021/acs.iecr.9b03159>.
- [52] N. De Vos, C. Maton, C.V. Stevens, Electrochemical stability of ionic liquids: general influences and degradation mechanisms, *ChemElectrochem* 1 (2014) 1258–1270, <https://doi.org/10.1002/celec.201402086>.
- [53] E. Jónsson, Ionic liquids as electrolytes for energy storage applications – a modelling perspective, *Energy Storage Mater.* 25 (2020) 827–835, <https://doi.org/10.1016/j.ensm.2019.08.030>.
- [54] M. Jiang, D. Zhu, X. Zhao, Electrolysis of ammonia for hydrogen production catalyzed by Pt and Pt-Ir deposited on nickel foam, *J. Energy Chem.* 23 (2014) 1–8, [https://doi.org/10.1016/s2095-4956\(14\)60110-8](https://doi.org/10.1016/s2095-4956(14)60110-8).
- [55] N.M. Adli, H. Zhang, S. Mukherjee, G. Wu, Review—ammonia oxidation electrocatalysis for hydrogen generation and fuel cells, *J. Electrochem. Soc.* 165 (2018) J3130–J3147, <https://doi.org/10.1149/2.0191815jes>.
- [56] C. Lian, H. Liu, C. Li, J. Wu, Hunting ionic liquids with large electrochemical potential windows, *AIChE J.* 65 (2018) 804–810, <https://doi.org/10.1002/aic.16467>.
- [57] N. Qorbani, A.H. Jalili, B. Adib, Anomalous high solubility behavior of methanethiol in alkylimidazolium-based ionic liquids, *J. Mol. Liq.* 350 (2022) 118529, <https://doi.org/10.1016/j.molliq.2022.118529>.
- [58] L. Yuan, X. Zhang, B. Ren, Y. Yang, Y. Bai, L. Bai, H. Gao, S. Zeng, Dual-functionalized protic ionic liquids for efficient absorption of NH₃ through synergistically physicochemical interaction, *J. Chem. Technol. Biotechnol.* 95 (2020) 1815–1824, <https://doi.org/10.1002/jctb.6381>.
- [59] J. Tian, B. Liu, Ammonia capture with ionic liquid systems: a review, *Crit. Rev. Environ. Sci. Technol.* 52 (2022) 767–809, <https://doi.org/10.1080/10643389.2020.1835437>.
- [60] A.H. Jalili, A. Mehdizadeh, A.N. Ahmadi, A.T. Zoghi, M. Shokouhi, Solubility behavior of CO₂ and H₂S in 1-benzyl-3-methylimidazolium bis(trifluoromethylsulfonyl)imide ionic liquid, *J. Chem. Thermodyn.* 167 (2022) 106721, <https://doi.org/10.1016/j.jct.2021.106721>.
- [61] Y. Cao, X. Zhang, S. Zeng, Y. Liu, H. Dong, C. Deng, Protic ionic liquid-based deep eutectic solvents with multiple hydrogen bonding sites for efficient absorption of NH₃, *AIChE J.* 66 (2020) 1–9, <https://doi.org/10.1002/aic.16253>.
- [62] W. Shi, E.J. Maginn, Molecular simulation of ammonia absorption in the ionic liquid 1-ethyl-3-methylimidazolium bis(trifluoromethylsulfonyl)imide ([emim][Tf₂N]), *AIChE J.* 55 (2009) 2414–2421, <https://doi.org/10.1002/aic.11910>.
- [63] M. Azadpour, Z. Jayhani, S. Pourmand, A. Mohebbi, Molecular dynamic insight into solubility of H₂S in ionic liquids [emim][BF₄], [emim][OTf] and [emim][Tf₂N], *J. Mol. Liq.* 338 (2021) 117114, <https://doi.org/10.1016/j.molliq.2021.117114>.
- [64] I.G. Economou, Statistical associating fluid theory: a successful model for the calculation of thermodynamic and phase equilibrium properties of complex fluid mixtures, *Ind. Eng. Chem. Res.* 41 (2002) 953–962, <https://doi.org/10.1021/ie0102201>.
- [65] A. Piña-Martínez, R. Privat, I.K. Nikolaidis, I.G. Economou, J.-N. Jaubert, What is the optimal activity coefficient model to be combined with the translated-consistent peng–robinson equation of state through advanced mixing rules? cross-comparison and grading of the wilson, uniquac, and nrtl ae models against a benchmark database involving 200 binary systems, *Ind. Eng. Chem. Res.* 60 (2021) 17228–17247, <https://doi.org/10.1021/acs.iecr.1c03003>.